JOURNAL OF SOLID STATE CHEMISTRY **124,** 374–380 (1996)
ARTICLE NO. 0252

# Synthesis, Structure, and Magnetic Properties of $CaMSi_2O_6$ ($M$ = Co, Ni) Compounds and Their Solid Solutions

G. Durand, S. Vilminot,[1] P. Rabu, A. Derory, and J. P. Lambour

*Groupe des Matériaux Inorganiques, IPCMS, UMR 46 CNRS, 23 rue du Loess, 67037 Strasbourg Cedex, France*

and

E. Ressouche

*CEA/Département de Recherche Fondamentale sur la Matière Condensée, SPSMS-MDN, 17 rue des Martyrs, 38054 Grenoble Cedex 9, France*

Received January 24, 1996; in revised form April 22, 1996; accepted April 25, 1996

**The title compounds have been synthesized using a sol–gel route from calcium and transition metal nitrates and tetraethylorthosilicate. A silica excess was used to avoid the formation of parasitic phases. These materials exhibit the clinopyroxene structure where the transition metal build $MO_6$ octahedra from infinite zigzag chains running in the $c$ axis direction. Magnetic and specific heat measurements demonstrate the existence of ferromagnetic interactions inside the $MO_6$ zigzag chains that order antiferromagnetically below $T_N$ = 9.75 and 20.2 K for $M$ = Co and Ni, respectively. Neutron powder diffraction data allow the determination of the magnitude, $m_0 = 3.30 \pm 0.15$ $\mu_B$, and orientation, angle of 41° with the $a$ axis, of the magnetic moments inside the structure.** 

## INTRODUCTION

The pyroxene structure is exhibited by natural minerals and has been the subject of many studies by geologists (1). Due to the presence of a mixture of different metals in the natural source, the corresponding pyroxenes always crystallize as solid solutions of different cations, mainly alkali, alkaline-earth, and transition metal cations. Therefore, geologists are interested in the relationships between crystal structure and the partitioning of transition metal ions among coexisting pyroxene-like compounds (2–4).

The pyroxene structure is characterized by the presence of infinite $(Si_2O_6)_\infty$ simple chains of corner-sharing $SiO_4$ tetrahedra. It crystallizes either in the *Pbca* orthorhombic space group defining the orthopyroxene family, with $(Mg, Fe)_2Si_2O_6$ as the parent compound, or in the $C2/c$ monoclinic space group, defining the clinopyroxene family, such as diopside $CaMgSi_2O_6$. The oxygen coordination polyhedra around the cations also build infinite chains. Although numerous studies have been devoted to crystal structure determinations in these families, few results have appeared on their magnetic properties. Ferrous chain silicates of the pyroxene group reveal (5) a collinear antiferromagnetic ordering below $T_N$ = 45, 26, and 35 K for $FeSiO_3$, $Fe_{0.87}Mg_{0.13}SiO_3$, and $CaFe_{0.8}Mg_{0.2}Si_2O_6$, respectively. The structures of cobalt and nickel clinopyroxenes, $CaCoSi_2O_6$ and $CaNiSi_2O_6$, are known (6), yet no magnetic characterizations have been reported on these compounds. This paper deals with the synthesis using a sol–gel route of $CaMSi_2O_6$ ($M$ = Co, Ni) samples and their solid solutions. The resulting compounds have been characterized by magnetic and specific heat measurements. Structure refinements have been performed to determine the relations between crystal structure and magnetic properties of $MO_6$ simple chains.

## EXPERIMENTAL

Both compounds have been prepared using a sol–gel route involving calcium nitrate, $Ca(NO_3)_2$, transition metal nitrates, $M(NO_3)_2 \cdot 6H_2O$ ($M$ = Co, Ni), and tetraethylorthosilicate (TEOS), $Si(OC_2H_5)_4$, as starting materials. After dissolution in ethanol, hydrolysis was promoted by dropwise addition of a water/$HNO_3$/ethanol (1/0.01/4 ratios) solution, to achieve a $H_2O$/Si ratio of 4. Gelation took place within 30 min at 50°C. The resulting gel was dried at 40°C overnight to remove most of the solvents before further thermal treatments. Starting from the constituents in stoichiometric proportions, it was difficult to obtain the pure phase, even after long duration annealings. An excess of silica promotes the formation of $CaMSi_2O_6$ phases and both compounds have been obtained after calcination at 1200°C for 48 h with Ca/M/Si in 1/1/4 respec-

[1] To whom correspondence should be addressed.



0022-4596/96 $18.00

tive proportions. The cobalt compound has a pink color, and the nickel one is green. On the other hand, Co–Ni solid solutions, $CaCo_{1-x}Ni_xSi_2O_6$ ($x$ = 0.25, 0.50, and 0.75), were obtained without silica excess using the same annealing conditions. The sol–gel route allows a good mixing of the starting oxides to be obtained without the grinding step. It also results in a decrease of the reaction temperatures.

X-ray diffraction patterns were recorded on a Siemens D500 diffractometer using monochromatized Co$K\alpha_1$ radiation. Susceptibility measurements were done on powder samples by means of a Manics Faraday-based magnetosusceptometer. Specific heat measurements were done using a quasi-adiabatic method (7). Neutron diffraction data were collected on the multichannel experiment DN5 at the Siloe reactor of the CEN-Grenoble.

## RESULTS AND DISCUSSION

### *Magnetic Measurements*

The temperature dependence of the magnetic susceptibility (recorded at 12,800 Oe) is plotted in Fig. 1. The presence of $SiO_2$ as a parasitic phase does not perturb the magnetic measurements. For the Ni sample, the magnetic susceptibility (Fig. 1) has a maximum at $T_N$ = 21.7 K and follows a Curie–Weiss law between 150 and 300 K. The positive $\theta$ value (Table 1) is related to ferromagnetic interactions as deduced from the small increase of $\chi T$ values in the domain 300–50 K (Fig. 1, inset). Below 50 K, the strong decrease of $\chi T$, with an inflection point at ≅24 K corresponding to the maximum of $\chi$, is likely related to a long-range antiferromagnetic order. As shown in Fig. 1 for $M$ = Co, $\chi$T slowly decreases between 300 and 50 K, and then a plateau ($\chi T \cong 2.5$ emu · K · mol$^{-1}$) is observed between 50 and 25 K. Such behavior may be related to the spin-orbit coupling effect for the Co(II) ion, that stabilizes a Kramers doublet ground state. However, the $\chi T$ value, 2.5 emu · K · mol$^{-1}$, appears to be higher than expected, 1.875 emu · K · mol$^{-1}$. Other effects are therefore to be considered in this part of the curve. At lower temperatures, $\chi T$ sharply decreases down to zero, in relation with antiferromagnetic interactions in this temperature domain, with a maximum at 10.0 K on the $\chi = f(T)$ curve. In the paramagnetic domain, the magnetic susceptibility follows a Curie–Weiss law with a negative $\theta$ value (Table 1).

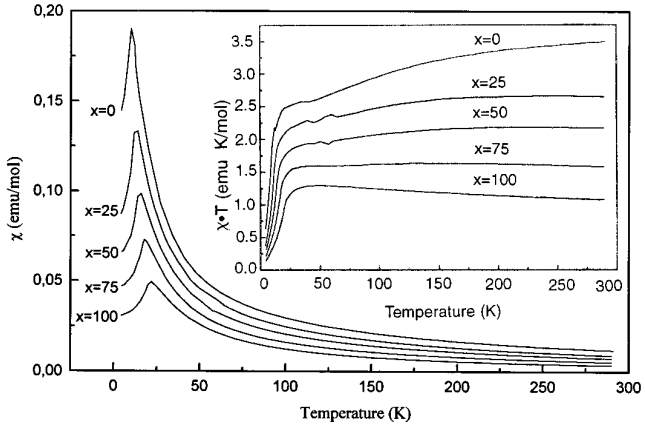


**FIG. 1.** Temperature dependence of the magnetic susceptibility and the $\chi T$ product for $CaCo_{1-x}Ni_xSi_2O_6$ solid solutions in an applied field of 12,800 Oe.

**TABLE 1**
**Magnetic Data of $CaCo_{1-x}Ni_xSi_2O_6$ Solid Solutions**

| $x$ | $T_N$ (K) | $C$ | $\theta$ (K) |
|---|---|---|---|
| 0.0 | 10.0 | 3.82 | −28 |
| 0.25 | 13.2 | 2.68 | −3 |
| 0.50 | 15.6 | 2.14 | 4 |
| 0.75 | 18.3 | 1.52 | 12 |
| 1.0 | 21.7 | 0.96 | 31 |

Similar results are observed for the solid solutions (Fig. 1) with a linear evolution of $T_N$ versus $x$ as expected from a solid solution (Table 1). As the cobalt content decreases, the spin–orbit coupling plateau progressively vanishes from the $\chi T$ curves.

### *Specific Heat Measurements*

Low temperature specific heat measurements reveal for both Co and Ni samples the presence of a λ-type anomaly at 9.75(±0.08) and 20.2(±0.4) K in agreement with the temperature of susceptibility maxima. The increase of Cp at higher temperature is mainly due to the phonon contribution (Fig. 2). These anomalies confirm the stabilization of a long-range magnetic ordering. The high temperature data have been fitted to the relationship $Cp = AT^{-2} + BT^3$, where the first term is ascribed to magnetic correlations while the second term deals with lattice contribution. After substracting the latter (full line in Fig. 2), we get the specific heat of magnetic origin (8). It also allows the determination of the magnetic entropy, $S_M$; the experimental value of $\Delta S_M$ associated with the magnetic transition (Fig. 3) agrees with the theoretical one given by the formula (8):

$$\Delta S_M = R\mathrm{Ln}(2S + 1) \quad \text{with} \quad S = \text{spin value.}$$

### *Structural Refinements*

As a long-range magnetic order has been evidenced at low temperature from specific heat data, neutron diffraction measurements have been performed on the Co sample. Structure refinements have been first performed from X-ray powder data.

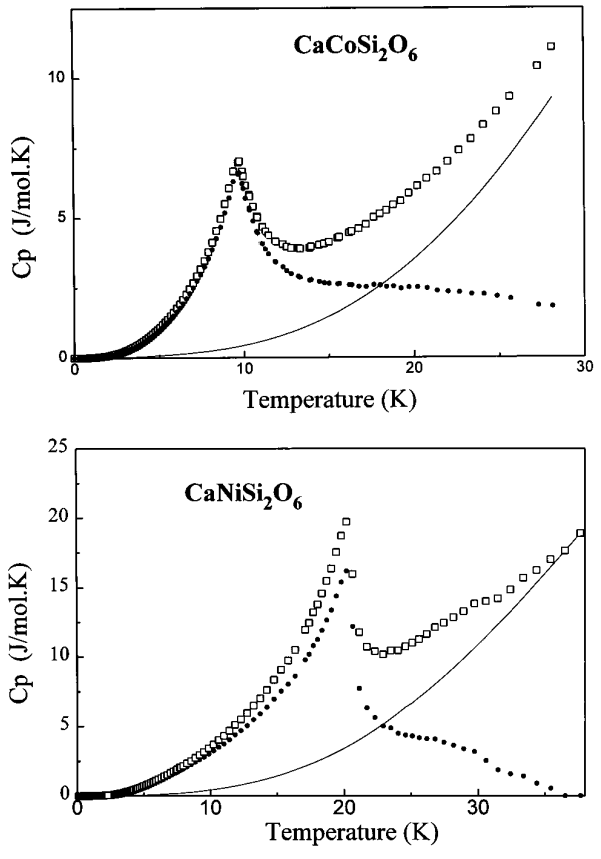


**FIG. 2.** Temperature dependence of the specific heat of $CaCoSi_2O_6$ and $CaNiSi_2O_6$. The full line and dotted line represent the lattice and magnetic contributions, respectively.

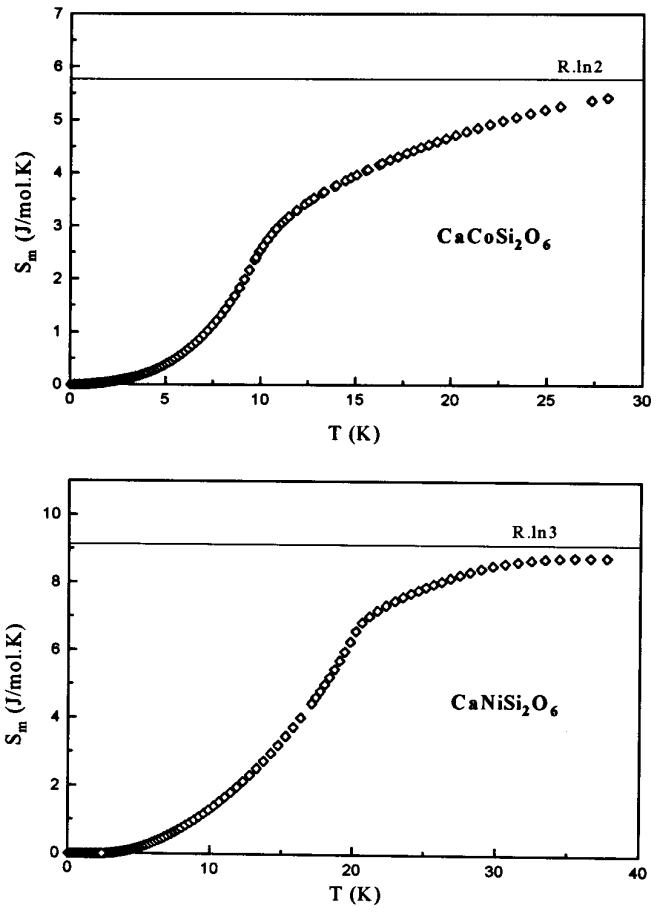


**FIG. 3.** Evolution of the magnetic entropy versus temperature.

*X-ray diffraction.* X-ray diffraction powder data have been collected at room temperature and the refinements were done starting from the data of Ghose *et al.* (6). The X-ray powder patterns were fitted to the calculated ones using a full-profile analysis program (Rietveld method, FULLPROF program (9)) to minimize the profile discrepancy factor

$$Rp = \sum_i y_i - y_{ci} \Big/ \sum_i y_i,$$

where $y_i$ and $y_{ci}$ are the observed and calculated values at the ith position, respectively. Calculations were performed in the *C*2/*c* monoclinic space group. Table 2 lists the refinement conditions.

As revealed by the discrepancy factors, the presence of $SiO_2$, mainly as tridymite, strongly disturbs the refinements, even excluding from the refinement $2\theta$ regions where the most intense $SiO_2$ lines appear ($23.50 < 2\theta < 32.50$). This influence is particularly important for the cobalt compound. Table 3 gives the final parameters and Table 4 lists some interatomic distances and angles.

The structure can be considered as build up by three kinds of infinite chains running in the *c* axis direction (Fig. 4):

—edge-sharing $MO_6$ octahedral zigzag chains, with the metal center at $x = 0$ and 1/2,

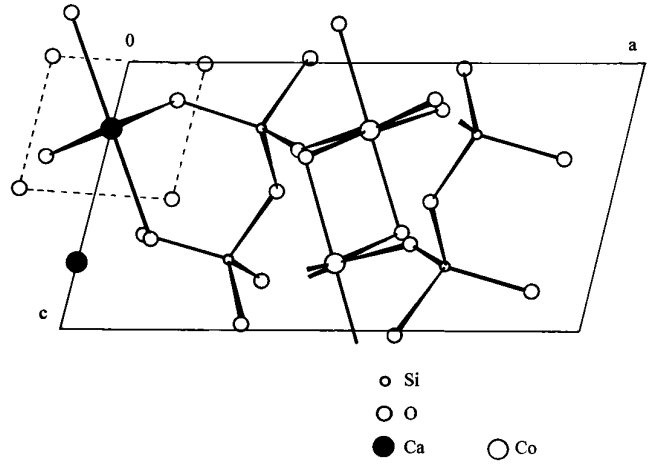


**FIG. 4.** Projection of the structure on the *ac* plane. For clarity, only 2 Ca atoms, 2 Co atoms, and 4 Si atoms with the oxygen atoms involved in their respective coordination polyhedra have been represented.

**TABLE 2**
**Refinement Conditions (X-Ray Powder Data) for $CaCo_{1-x}Ni_xSi_2O_6$ Samples**

| | $x = 0$ | $x = 0.25$ | $x = 0.50$ | $x = 0.75$ | $x = 1$ |
|---|---|---|---|---|---|
| $a$(Å) | 9.7970(4) | 9.7832(3) | 9.7673(4) | 9.7514(4) | 9.7355(4) |
| $b$(Å) | 8.9577(4) | 8.9429(3) | 8.9290(3) | 8.9163(3) | 8.9025(3) |
| $c$(Å) | 5.2445(2) | 5.2397(2) | 5.2351(2) | 5.2313(2) | 5.2272(2) |
| $\beta$(°) | 105.513(3) | 105.594(3) | 105.698(3) | 105.777(2) | 105.839(2) |
| $Z$ | 4 | 4 | 4 | 4 | 4 |
| Space group | $C2/c$ | $C2/c$ | $C2/c$ | $C2/c$ | $C2/c$ |
| $2\theta$ range | 10–110 | 10–100 | 10–100 | 10–100 | 10–110 |
| Step scan °$2\theta$ | 0.02 | 0.02 | 0.02 | 0.02 | 0.02 |
| Range of calc. profile in FWHM units | 3.5 | 3.5 | 3.5 | 3.5 | 3.5 |
| Reflection number | 156 | 162 | 160 | 162 | 158 |
| Profile parameter number | 12 | 12 | 12 | 12 | 12 |
| Atom number | 6 | 6 | 6 | 6 | 6 |
| RF(%) | 13.5 | 7.0 | 7.4 | 5.8 | 10.4 |
| RB(%) | 13.2 | 8.4 | 7.5 | 6.7 | 9.6 |
| Rp(%) | 29.2 | 21.4 | 19.9 | 18.0 | 22.3 |

—edge-sharing $CaO_8$ polyhedral chains, at the same $x$ position and shifted along the $b$ axis direction with regard to the $MO_6$ chains,

—corner-sharing $SiO_4$ tetrahedral chains, running between the previous metal oxide chains.

The $MO_6$ octahedra are slightly distorted, the distortion increasing with the amount of nickel. The differences between the shortest and the longest $M$–O bond distances vary from 0.31 to 0.146 Å for $x = 0$ and $x = 1$, respectively. The average angular deviations from an ideal octahedral

**TABLE 3**
**Refined Structural Parameters for $CaCo_{1-x}Ni_xSi_2O_6$ Samples**

| Atom | | $x = 0$ | $x = 0.25$ | $x = 0.50$ | $x = 0.75$ | $x = 1$ |
|---|---|---|---|---|---|---|
| $M$ | $x/a$ | 0 | 0 | 0 | 0 | 0 |
| | $y/b$ | 0.9090(7) | 0.9080(5) | 0.9088(5) | 0.9079(5) | 0.9061(5) |
| (4$e$) | $z/c$ | 0.25 | 0.25 | 0.25 | 0.25 | 0.25 |
| | $B$(Å$^2$) | 2.0(2) | 2.0(2) | 2.2(2) | 1.8(1) | 1.8(1) |
| Ca | $x/a$ | 0 | 0 | 0 | 0 | 0 |
| | $y/b$ | 0.2956(8) | 0.2983(7) | 0.2951(7) | 0.2962(7) | 0.2956(6) |
| (4$e$) | $z/c$ | 0.25 | 0.25 | 0.25 | 0.25 | 0.25 |
| | $B$(Å$^2$) | 3.9(3) | 3.9(2) | 3.6(2) | 3.3(2) | 3.6(2) |
| Si | $x/a$ | 0.2891(6) | 0.2868(6) | 0.2878(6) | 0.2867(5) | 0.2861(5) |
| | $y/b$ | 0.0919(8) | 0.0973(7) | 0.0946(7) | 0.0927(6) | 0.0915(6) |
| (8$f$) | $z/c$ | 0.2349(12) | 0.2310(11) | 0.2332(12) | 0.2309(10) | 0.2280(10) |
| | $B$(Å$^2$) | 2.5(2) | 2.3(2) | 3.2(2) | 2.9(2) | 3.2(2) |
| O1 | $x/a$ | 0.1124(10) | 0.1150(10) | 0.1139(11) | 0.1144(9) | 0.1146(9) |
| | $y/b$ | 0.0872(14) | 0.0826(14) | 0.0875(15) | 0.0872(13) | 0.0829(13) |
| (8$f$) | $z/c$ | 0.1443(20) | 0.1496(20) | 0.1433(23) | 0.1402(18) | 0.1390(17) |
| | $B$(Å$^2$) | 3.0(3) | 2.9(3) | 4.3(4) | 3.0(3) | 3.1(3) |
| O2 | $x/a$ | 0.3639(13) | 0.3647(10) | 0.3637(11) | 0.3658(10) | 0.3693(9) |
| | $y/b$ | 0.2448(14) | 0.2507(13) | 0.2506(14) | 0.2516(12) | 0.2558(11) |
| (8$f$) | $z/c$ | 0.3199(24) | 0.3184(20) | 0.3245(24) | 0.3207(18) | 0.3231(16) |
| | $B$(Å$^2$) | 3.2(4) | 2.8(4) | 3.9(4) | 2.9(3) | 1.9(3) |
| O3 | $x/a$ | 0.3491(11) | 0.3483(10) | 0.3510(10) | 0.3474(9) | 0.3457(9) |
| | $y/b$ | 0.0190(11) | 0.0167(10) | 0.0187(11) | 0.0198(10) | 0.0179(9) |
| (8$f$) | $z/c$ | −0.0204(27) | −0.0128(28) | −0.0055(28) | −0.0087(25) | −0.0151(23) |
| | $B$(Å$^2$) | 2.3(3) | 1.5(3) | 2.2(3) | 2.0(3) | 1.8(2) |

**TABLE 4**
**Interatomic Distances (Å) and Angles (°)**

| | $x = 0$ | $x = 0.25$ | $x = 0.50$ | $x = 0.75$ | $x = 1$ |
|---|---|---|---|---|---|
| | | | Ca Polyhedron | | |
| Ca–O(1) (2) | 2.309(13) | 2.363(13) | 2.307(14) | 2.323(12) | 2.350(12) |
| Ca–O(2) (2) | 2.321(12) | 2.334(10) | 2.301(12) | 2.311(9) | 2.293(8) |
| Ca–O(3) (2) | 2.661(13) | 2.611(12) | 2.615(12) | 2.632(11) | 2.638(10) |
| Ca–O(3) (2) | 2.710(12) | 2.734(12) | 2.744(12) | 2.742(11) | 2.744(10) |
| Mean Ca–O | 2.500 | 2.511 | 2.492 | 2.502 | 2.506 |
| Mean Ca–O[6] | 2.502 | — | — | — | 2.496 |
| | | | *M* octahedron | | |
| *M*–O(1) (2) | 2.096(13) | 2.073(12) | 2.105(13) | 2.116(11) | 2.101(11) |
| *M*–O(1) (2) | 2.067(10) | 2.095(10) | 2.059(12) | 2.043(9) | 2.037(9) |
| *M*–O(2) (2) | 2.083(14) | 2.028(11) | 2.050(12) | 2.014(11) | 1.955(10) |
| Mean *M*–O | 2.082 | 2.065 | 2.071 | 2.058 | 2.031 |
| Mean *M*–O[6] | 2.101 | — | — | — | 2.070 |
| O(1)–*M*–O(1) | 80.8(7) | 82.3(7) | 81.4(7) | 81.9(6) | 82.9(6) |
| O(1)–*M*–O(1) (2) | 94.3(8) | 92.4(7) | 94.1(9) | 94.0(7) | 93.0(7) |
| O(1)–*M*–O(1) (2) | 84.3(7) | 84.2(7) | 84.5(8) | 84.1(6) | 82.9(6) |
| O(1)–*M*–O(2) (2) | 172(1) | 173(1) | 172(1) | 172(1) | 172(1) |
| O(1)–*M*–O(2) (2) | 94.9(9) | 93.0(8) | 93.1(9) | 93.2(8) | 92.0(8) |
| O(1)–*M*–O(1) | 178(1) | 175(2) | 178(2) | 178(2) | 174(2) |
| O(1)–*M*–O(2) (2) | 91.7(8) | 90.2(7) | 91.4(8) | 92.1(7) | 92.6(7) |
| O(1)–*M*–O(2) (2) | 89.6(8) | 84.2(8) | 89.9(8) | 89.6(7) | 91.1(6) |
| O(2)–*M*–O(2) | 90.1(9) | 92.2(8) | 92.9(8) | 92.4(7) | 93.6(7) |
| | | | Si tetrahedron | | |
| Si–O(1) | 1.669(12) | 1.624(12) | 1.636(13) | 1.618(11) | 1.608(10) |
| Si–O(2) | 1.561(14) | 1.576(13) | 1.590(14) | 1.621(12) | 1.680(11) |
| Si–O(3) | 1.728(14) | 1.711(14) | 1.679(14) | 1.658(12) | 1.668(12) |
| Si–O(3) | 1.605(14) | 1.664(14) | 1.679(14) | 1.666(13) | 1.632(12) |
| Mean Si–O | 1.641 | 1.644 | 1.646 | 1.641 | 1.647 |
| Mean Si–O[6] | 1.636 | — | — | — | 1.637 |
| O(1)–Si–O(2) | 118.4(16) | 122.1(16) | 118.9(16) | 119.1(14) | 120.4(13) |
| O(1)–Si–O(3) | 108.2(12) | 108.5(12) | 109.4(13) | 108.8(11) | 108.1(11) |
| O(1)–Si–O(3) | 110.0(13) | 106.6(12) | 109.6(14) | 109.4(12) | 108.5(11) |
| O(2)–Si–O(3) | 108.8(14) | 110.1(13) | 110.0(14) | 108.8(12) | 109.1(11) |
| O(2)–Si–O(3) | 105.7(14) | 104.9(12) | 104.1(13) | 104.7(11) | 104.0(10) |
| O(3)–Si–O(3) | 104.9(14) | 102.8(13) | 103.6(14) | 105.2(13) | 105.8(12) |
| Si–O(3)–Si | 136.5(19) | 136.5(18) | 136.2(18) | 137.2(17) | 137.9(16) |

angle vary between 3.9° ($x = 0$, 0.25 and 0.5) and 4.3° ($x = 1$). As expected, the *M*–O bond length decreases from cobalt to nickel, even if a value higher than expected is observed for $x = 0.5$.

The $CaO_8$ polyhedron is an irregularly shaped trigonal bipyramid, with four nearest oxygen neighbors along the axial (Ca–O(2) = 2.318 Å) and two equatorial (Ca–O(1) = 2.327 Å) directions. In the last equatorial direction, four oxygen atoms, at the corners of a 2.65–2.95 Å parallelogram, define longer Ca–O bonds (2.65 and 2.72 Å). The polyhedra are linked by sharing the 2.95 Å edge of the parallelogram.

The $SiO_4$ tetrahedra are distorted, probably in relation with the quality of the recorded diffraction patterns. The distortion, estimated by the difference between the shortest and the longest Si–O bond distances, varies in the opposite way than that observed for the corresponding $MO_6$ octahedron: a more regular $SiO_4$ tetrahedron is associated to a more distorted $MO_6$ octahedron.

The structure refinements performed from X-ray diffraction data allowed one to find the general features presented in reference (6). However, much caution has to be taken if one considers the details of the bond lengths and angles, some variations being in relation with the limitation of the technique. So, in the case of corner-sharing $SiO_4$ tetrahedra, there is a well established inverse correlation between mean Si–O bond lengths and the Si–O–Si angle. This relation is only fullfilled in the case of the Co–Ni solid solutions

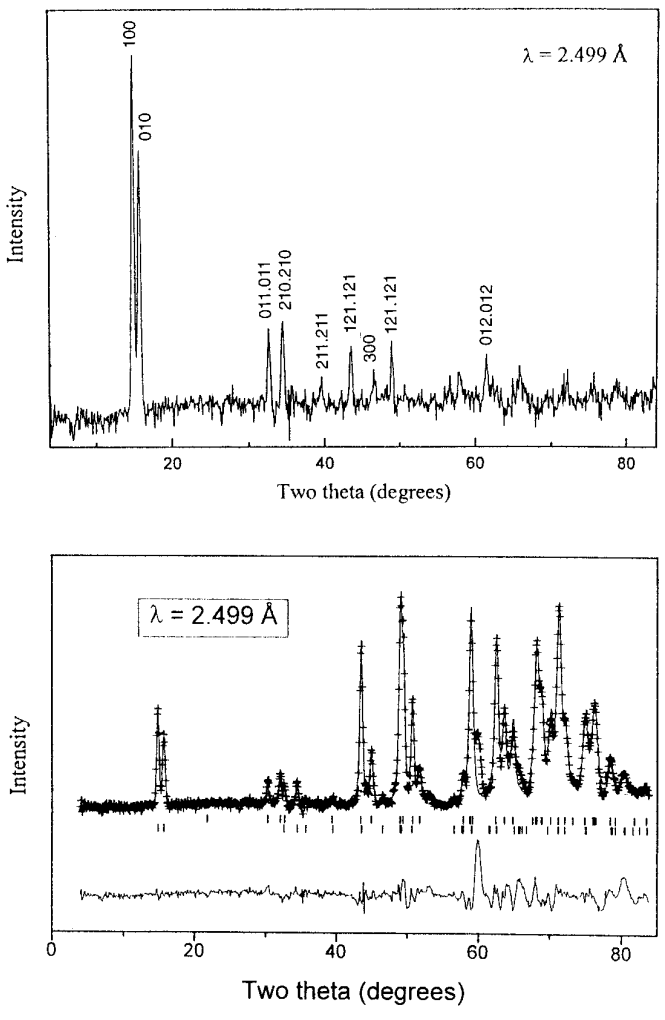


**FIG. 5.** Neutron diffraction pattern of $CaCoSi_2O_6$ at 2 K: difference pattern 15–2 K (top), observed, calculated, and difference profiles after refinement, first line of markers: nuclear lines, second line of markers: magnetic lines (bottom).

($x$ = 0.25, 0.50, and 0.75), while the values for the Co and Ni compounds are outside the expected evolution (Table 4). These results can also be related to the presence of an excess of silica.

*Neutron diffraction.* Neutron diffraction patterns were recorded at different temperatures on the same $CaCoSi_2O_6$ powder previously used for X-ray measurements.

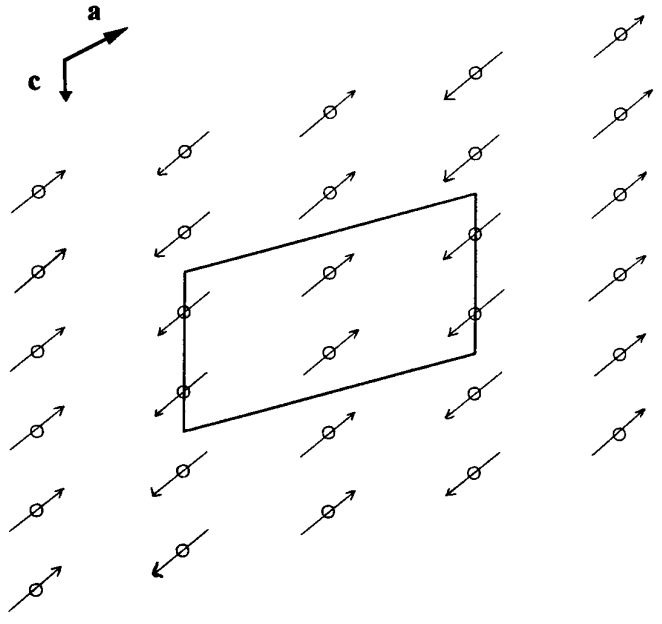


**FIG. 6.** Schematic illustration of the magnetic moment arrangement.

As expected from magnetic and specific heat measurements, additional reflections appear at temperatures below $T_N$ = 10 K (Fig. 5). These reflections, such as (100), (010), (210), (211), (121), can be indexed using the same unit cell as for the nuclear reflections.

The first refinement was performed by only considering the nuclear contribution. The resulting cell constants and atomic parameters are given in Table 5.

As previously discussed by Wiedenmann and Regnard (5) in the case of isostructural hedenbergite, $CaFe_{0.8}Mg_{0.2}Si_2O_6$, the following considerations must be taken into account to analyze the magnetic structure:

—The magnetic reflections are associated with a [010] wavevector;

—This wavevector, symmetry point in the first Brillouin zone, defines a collinear ordering of the magnetic moments inside a $CoO_6$ chain;

**TABLE 5**
**Results of a Rietveld Powder Refinement of $CaCoSi_2O_6$ Measured at 2 K, Space Group $C2/c$**

| Atom | Position | $x/a$ | $y/b$ | $z/c$ | |
|---|---|---|---|---|---|
| Co | 4*e* | 0 | 0.890(3) | 0.25 | $a$ = 9.786(2) |
| Ca | 4*e* | 0 | 0.299(2) | 0.25 | $b$ = 8.944(2) |
| Si | 8*f* | 0.286(2) | 0.077(2) | 0.251(6) | $c$ = 5.242(1) |
| O1 | 8*f* | 0.110(1) | 0.096(1) | 0.155(3) | RB (%) = 7.56 |
| O2 | 8*f* | 0.357(1) | 0.248(2) | 0.325(3) | RF (%) = 5.14 |
| O3 | 8*f* | 0.356(1) | 0.018(2) | −0.010(3) | Rp (%) = 16.1 |

—Moreover, the observation of reflections ($h00$) and ($h0l$) with $l = 2n$ implies that these moments must be ferromagnetically coupled;

—From one chain to the next, the magnetic moments must be antiparallel;

—The observation of ($0k0$) reflections with $k = 2n + 1$ implies that the moments cannot be aligned along the $b$ axis;

—Application of group theory leaves as the only possibility an alignment of the moments within the $ac$ plane.

The magnetic structure has therefore been refined according to these considerations using the FULLPROF program. It yields $m_x = 1.91 \pm 0.23\ \mu_B$ and $m_z = -2.23 \pm 0.12\ \mu_B$, corresponding to $m_0 = 3.30 \pm 0.15\ \mu_B$ and to an angle $\alpha = 41°$, between $m$ and the $a$ axis. Figure 6 gives a schematic picture of the magnetic moment arrangement.

The neutron diffraction results therefore confirm the magnetic and specific heat measurements. In the case of the nickel sample, the slight increase of the $\chi T$ value from room temperature down to 30 K is related to ferromagnetic coupling inside the $NiO_6$ zigzag chains. Such coupling takes place from two superexchange pathways via oxygen O(1) bridges with $Ni \cdots Ni' = 3.103$ Å. In the case of the cobalt compound, we noticed that the $\chi T$ value in the temperature domain of the plateau related to the existence of a Kramers doublet ground state, i.e., between 50 and 25 K, was higher than expected. Such a deviation can therefore be explained by a contribution of a ferromagnetic coupling between Co atoms inside the $CoO_6$ infinite chains.

## CONCLUSION

A series of solid solutions, $CaCo_{1-x}Ni_xSi_2O_6$, exhibiting the clinopyroxene structure has been synthesized using a sol–gel route from calcium and transition metal nitrates and TEOS. These materials exhibit a structure built up by three kinds of infinite chains, i.e., edge-sharing $MO_6$ octahedral chains, edge-sharing $CaO_8$ polyhedral chains, and corner-sharing $SiO_4$ tetrahedral chains. The presence of infinite chains of transition metal in the structure suggested a study of the magnetic behavior of these entities. Magnetic and specific heat measurements demonstrated the existence of ferromagnetic interactions inside the $MO_6$ chains that order antiferromagnetically to each other at low temperature. These conclusions have been clearly confirmed from neutron diffraction data which allow the determination of the orientation and magnitude of the magnetic moments inside the structure.

## REFERENCES

1. Crystal chemistry of silicate pyroxenes. Mineralogical Society of America Reviews of Mineralogy, 7 (1980).
2. S. Ghose and C. Wan, *EOS* **56,** 1076 (1975).
3. P. H. Ribbe and A. R. Prunier Jr., *Am. Mineral.* **62,** 710 (1977).
4. M. Cameron and J. J. Papike, *Am. Mineral.* **66,** 1 (1981).
5. A. Wiedenmann and J.-R. Regnard, *Solid State Comm.* **57,** 499 (1986)
6. S. Ghose, C. Wan and F. P. Okamura, *Am. Mineral.* **72,** 375 (1987).
7. The calorimeter was designed by R. Kuentzler and Y. Dossmann (Strasbourg) for measurements in the temperature range 0.9–40 K. It is made of an adiabatic chamber with a saphire sample holder, equipped with a Ge resistance thermometer and an evaporation deposit Cr/Ti heater. The sample holder is suspended with nylon threads. The accuracy of the measurements is better than 1%.
8. R. L. Carlin, "Magnetochemistry," p. 165. Springer-Verlag, Berlin/Heidelberg, 1986.
9. J. Rodriguez-Carvajal, "(I. L. L. Grenoble) Fullprof Program," Version 2.4.2, Dec. 1993. Original code provided by D. B. Wiles, R. A. Young, and A. Sakthivel.